Structure of the Crystalline Bilayer in the Subgel Phase of Dipalmitoylphosphatidylglycerol†

Allen E. Blaurock

Department of Biochemistry, University of North Carolina, Chapel Hill, North Carolina 27514

Thomas J. McIntosh*

Anatomy Department, Duke University Medical Center, Durham, North Carolina 27712

Received May 13, 1985

ABSTRACT: The structure of the subgel phase of dipalmitoylphosphatidylglycerol (DPPG) has been analyzed by X-ray diffraction techniques. Diffraction recorded from highly oriented DPPG specimens in the subgel phase extends to 2-Å resolution. There are sharp lamellar reflections on the meridian, and other reflections lie on a series of wide-angle lattice lines parallel to the meridian and crossing the equator in the range of 8–2 Å. The wide-angle lattice lines consist of radially sharp reflections centered on the equator of the X-ray film and also a series of broader, off-equatorial maxima. The lattice lines indicate that the DPPG molecules in each bilayer crystallize in a two-dimensional oblique lattice with dimensions a = 5.50 Å, b = 7.96 Å, and γ = 100.5°. These oblique lattices are not regularly aligned from bilayer to bilayer. Analysis of the lamellar diffraction shows that the bilayer has about the same thickness in the subgel and gel ($L_{\beta'}$) phases. In the direction normal to the hydrocarbon chains, the chains are significantly closer together in the subgel phase as compared to the normal $L_{\beta'}$ gel phase but have about the same separation as the chains in polyethylene and the crystalline *n*-alkanes. The bilayer thickness, area per lipid molecule, and intensity distribution along the lattice lines all indicate that in the subgel phase the hydrocarbon chains are tilted between 30 and 35° from the normal to the bilayer plane. Our analysis indicates that in the subgel phase the lateral packing of chains is much the same as in simple long-chain hydrocarbons such as polyethylene and crystalline *n*-alkanes, whereas the influence of the DPPG head group causes the chains to tilt relative to the bilayer normal.

Upon incubation at low temperatures, usually near 0 °C, the normal gel phase of many phospholipids converts to a stable "subgel" phase. The subgel phase has been studied by X-ray diffraction techniques for a number of phospholipids, including symmetric and mixed-chain phosphatidylcholines (Fuldner, 1981; Ruocco & Shipley, 1982; Stumpel et al., 1983), phosphatidylethanolamines (Seddon et al., 1983; Mulukutla & Shipley, 1984), and phosphatidylglycerol (Wilkinson & McIntosh, 1986). In each of these cases, the subgel phase is characterized by orders of a lamellar repeat period and several additional wide-angle reflections, some sharp and some broad, in the range of 8–2 Å. Although each of these studies concluded that the subgel phase is a more highly ordered phase than the normal $L_{\beta'}$ gel phase, details of molecular organization such as hydrocarbon chain packing mode, unit cell dimensions, and degree of chain tilt have not been established.

In the present study we have obtained X-ray diffraction patterns from highly oriented specimens of dipalmitoylphosphatidylglycerol. In these patterns the wide-angle reflections are observed to lie along vertical lines. The intensity varies continuously along each line rather than being restricted to discrete lattice points spaced evenly along the line. A typical line consists of a sharp equatorial reflection and broader off-equatorial maxima. These lines index as a simple and unique set of lattice lines arising from an oblique two-dimensional lattice with dimensions a = 5.50 Å, b = 7.96 Å, and γ = 100.5°. The area per unit cell is 43.0 Å^2. Swelling experiments have been used to obtain phase angles for the lamellar intensity data, which are used to calculate electron-density profiles at moderate resolution (12 Å) across the bilayer. The bilayer thickness, area per lipid molecule, and intensity distribution along the lattice lines all indicate that in the subgel phase the hydrocarbon chains tilt by 30–35°, which is similar to the chain tilt in the $L_{\beta'}$ phase. Our data indicate that the subgel phase is more highly ordered than the normal gel phase, with the hydrocarbon chains being closer together by about 0.4 Å.

Materials and Methods

DPPG[1] ammonium salt was used as obtained from Sigma Chemical Co., St. Louis, MO. Lipid suspensions were prepared by weighing dry lipid into small conical glass containers and adding a measured amount of 50 mM sodium phosphate buffer, pH 7.0. The buffer concentration was 20–60% by weight. The specimens were extensively vortexed, allowed to equilibrate at 60 °C for several hours, and then incubated at 4 °C for at least 2 weeks.

For some experiments, lipid suspensions were sealed in thin-wall X-ray capillary tubes and mounted in a temperature-regulated specimen holder in a pinhole collimation X-ray camera containing three sheets of Kodak DEF-5 X-ray film in a flat film cassette. Oriented specimens were prepared by adding a small amount of water to the suspension and then placing a drop of this diluted suspension in an X-ray capillary

† This work was supported by a grant from the National Institutes of Health (GM 27278). Support from the U.S. Public Health Service in the form of a shared instrumentation grant (RR 01964) is also gratefully acknowledged.

[1] Abbreviations: DPPG, L-α-dipalmitoylphosphatidylglycerol; DPPC, L-α-dipalmitoylphosphatidylcholine; DPPE, L-α-dipalmitoylphosphatidylethanolamine.

0006-2960/86/0425-0299$01.50/0

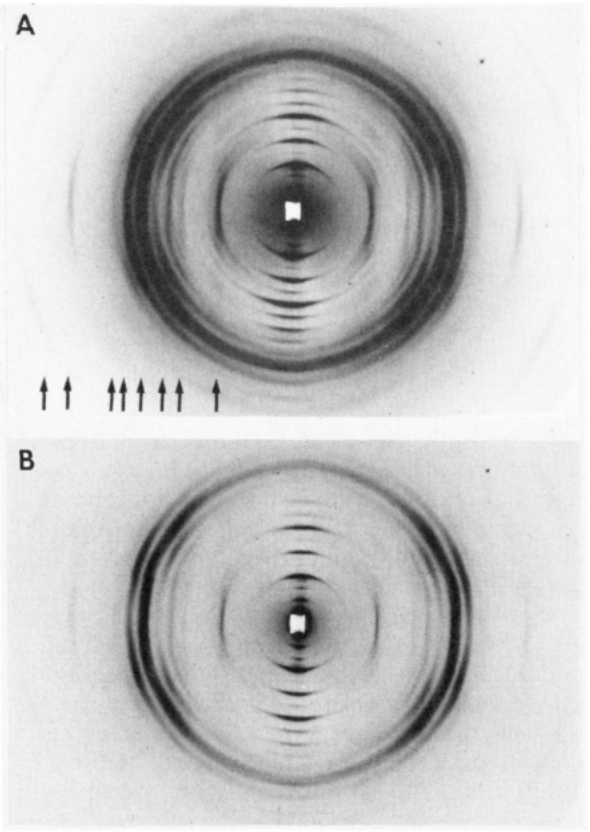

FIGURE 1: X-ray diffraction pattern of DPPG subgel phase oriented by partial dehydration in a capillary tube at 4 °C. In (A), 14 lamellar orders of a repeat period of 51.3 Å are visible on the meridian, the vertical axis through the center of the pattern. The arrows point to eight vertical wide-angle lattice lines described in the text. These are indexed as in Figure 2. (B) is the second X-ray film of the same exposure, showing more detail in the third, fourth, and fifth lattice lines.

tube. The tube was left open at both ends in a cold room in a high-humidity atmosphere and allowed to equilibrate (Blaurock, 1982). Oriented patterns were recorded on X-ray film with a Franks-type double-mirror X-ray camera and a GX-13 rotating anode X-ray generator. Specimen to film distances were from 4 to 10 cm, and exposure times were from 5 to 24 h. X-ray films were processed by standard techniques and densitometered with a Joyce-Loebl microdensitometer, Model MKIIIC. The background curve was subtracted, and integrated intensities of the lamellar reflections, $I(h)$, where h is the diffraction order, were obtained by measuring the areas under the corresponding densitometer peaks. For the unoriented specimens, the structure amplitude for each order of index h was set equal to $[h^2I(h)]^{1/2}$. The phase information for each diffraction order was determined as described under Results, and one-dimensional electron-density profiles were calculated by standard methods as previously described (McIntosh, 1978).

RESULTS

X-ray Patterns. An X-ray diffraction pattern from a highly oriented subgel DPPG specimen is shown in Figure 1. On the meridian the pattern contains 14 orders of a lamellar periodicity of 51 Å. There are also a number of additional wide-angle reflections that are observed at intervals along vertical lines parallel to the meridian, called lattice lines (arrows). The sharpest reflections, at 7.83, 5.42, 4.89, 4.11, 3.52, and 2.94 Å, are centered on the horizontal axis or equator of the pattern, whereas the broader reflections are located off the equator. For example, the first lattice line (arrow closest to center of pattern) consists of a radially sharp reflection at 7.83 Å centered on the equator and increasingly broad bands off of the equator at 7.44, 6.97, 6.38, 5.84, 5.02, 4.41, and 3.24 Å (see Table II). Similarly, the second lattice line (second arrow from center of pattern) consists of a radially sharp equatorial reflection at 5.42 Å and off equatorial bands at 5.25, 5.02, and 4.77 Å; the third lattice line consists of a radially sharp equatorial reflection at 4.89 Å and broader off-equatorial bands at 4.75, 4.42, and 4.05 Å; the fourth lattice line consists of a radially sharp equatorial reflection at 4.11 Å and a broader off-equatorial band at 4.00 Å; the sixth lattice line consists of a fairly sharp equatorial reflection at 3.52 Å and no off-equatorial bands; and the seventh lattice line contains a radially sharp equatorial reflection at 2.94 Å with no off-equatorial bands visible. Two of the vertical lines, the fifth and eighth in order from the center, are unusual in that these lines contain no sharp equatorial reflection, only broad off-equatorial bands. In the fifth lattice line, the broad bands are at 3.75, 3.56, 3.27, and 2.92 Å, and the lattice line on which those reflections lie crosses the equatorial axis at 3.92 Å. In the eighth lattice line the broad bands are at 2.50 and 2.40 Å, and these bands are assigned tentatively to a lattice line that crosses the equatorial axis at 2.65 Å. One other weak lattice line is observable on the original film at a larger distance from the center and is given in Table II. The most intense of all these wide-angle reflections, namely, the sharp reflections at 7.83, 5.42, 4.89, 4.11, and 2.94 Å and the broader bands at 4.75, 4.41, 4.00, and 3.75 Å, were observed as rings (in unoriented patterns) or long arcs (in partially oriented patterns) in the accompanying paper (Wilkinson & McIntosh, 1986). Note that some of the rings in the unoriented pattern represent more than one reflection. That is, a ring at about 4.75 Å would be generated by reflections at 4.77 and 4.75 Å (Table II); the ring at 4.41 Å is generated by reflections at 4.41 and 4.42 Å; and the ring at 4.00 Å, by reflections at 4.00 and 4.05 Å.

Analysis of Wide-Angle Diffraction. The diffraction pattern in Figure 1 is of the kind observed from the purple membrane (Blaurock & Stoeckenius, 1971). The vertical lattice lines of intensity in Figure 1 arise from planar arrays of diffracting units, in this case single lipid bilayers with the lipid molecules crystallized in two dimensions only. The diffracted intensity from such arrays varies continuously along lines perpendicular to the plane of the bilayer [see Figure 1 by Henderson & Unwin (1975)] rather than being confined to lattice points only, as is the case for three-dimensional diffracting arrays. The continuous intensity distribution along each line depends on the packing and internal structure of the diffracting unit in the planar array. The points at which the lattice lines cross the equator are the reciprocal lattice points given by $h\cdot\vec{a}^* + k\cdot\vec{b}^*$, where $\vec{a}^*$ and $\vec{b}^*$ are the reciprocal lattice vectors of the array. Thus, in the diffraction pattern of Figure 1, eight reciprocal lattice points are located along the equator with a ninth visible on the original film. Table I shows that an oblique lattice with $a = 5.50$ Å, $b = 7.96$ Å, and $\gamma = 100.5°$ predicts very closely eight of the nine reciprocal lattice points. As shown in Table II, there is an ambiguity in lattice-line assignment for two of the reflections, and the corresponding lattice point therefore has been omitted from Table I. Three of the eight points in Table I were needed to determine a, b, and γ, and thus, the test of our choice of lattice is its ability to predict the five remaining points. It does this with an error of 0.57%. In addition, this indexing is economical as all of the first seven predicted lattice points are observed and there are no unindexed lattice points in the pattern. The unit-cell area of this oblique lattice is 43.0 Å^2, somewhat less than the

Table I: Reciprocal Lattice in the DPPG Subgel Phase

lattice-line indices	Bragg spacings of lattice lines (Å) obsd[a]	calcd
(0, 1)	7.83	7.830[b]
(1, 0)	5.40	5.400[b]
(1, −1)	4.88	4.880
(1, 1)	4.11	4.110[b]
(0, 2)	(3.96)[a]	3.914
(1, −2)	3.51	3.484
(1, 2)	2.94	2.928
(1, 3)	2.21	2.199

[a] Bragg spacings of reflections centered on the in-plane axis, except for (0, 2), where only off-axis maxima are observed. [b] These three values were assumed in order to derive the unit-cell dimensions of a = 5.495 Å, b = 7.959 Å, and γ = 100.45°. The other five reflections were used to test the choice of this lattice and gave an rms error of predicted spacings of 0.028 Å, corresponding to 0.57% error.

Table II: Principal Maxima along Lattice Lines from DPPG Subgel Phase

lattice-line indices	Bragg spacing (Å)[a]	reciprocal distance from in-plane axis (Å^{-1})[b]
(0, 1)	7.83	0.000
	7.44	0.044
	6.97	0.066
	6.38	0.092
	5.84	0.115
	5.02	0.153
	4.41	0.188
	3.24	0.282
(1, 0)	5.42	0.000
	5.25	0.047
	5.02	0.075
	4.77	0.100
(1, −1)	4.89	0.000
	4.75	0.050
	4.42	0.096
	4.05	0.139
(1, 1)	4.11	0.000
	4.00	0.059
(0, 2)	3.75	0.081
	3.56	0.119
	3.27	0.169
	2.92	0.229
(1, −2)	3.52	0.000
(1, 2)	2.94	0.000
(0, 3)	2.50[c]	0.113
	2.40[c]	0.165
(1, 3)	2.21	0.000

[a] Measured on different pattern from Table I; small discrepancies with Table I are within rms error of measurement. [b] Calculated assuming reciprocal Bragg spacing in middle column as hypotenuse of right triangle with one side equal to reciprocal spacing of lattice line. [c] Probable lattice-line assignment; alternative possible assignments are to (2, 0) or (2, 1) lines.

area per lipid molecule for a gel-state lipid with tilted hydrocarbon chains [Tardieu et al. (1973) and see below].

There are two oblique two-dimensional space groups, number 1 with $p1$ symmetry and number 2 with $p2$ symmetry (Hahn, 1983). Since the unit-cell area implies that there is not sufficient room for two molecules to be placed side by side in the unit cell, a DPPG molecule would have to lie on a 2-fold axis for the space group to be $p2$. However, this is unlikely since the DPPG molecule itself does not have a 2-fold axis. Therefore, the space group is probably $p1$.

The off-equatorial diffraction along the lattice lines in Figure 1 consists of a series of intensity maxima, with the maxima becoming wider radially and also more arced farther away from the equator. The minimum wavelength principal (Bragg

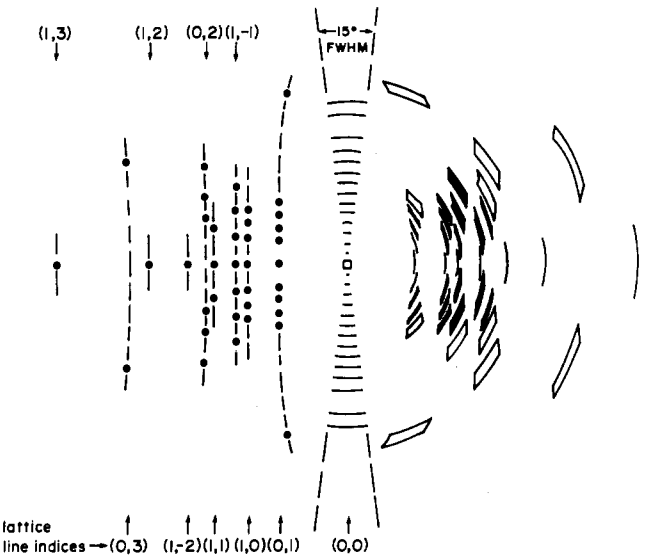

FIGURE 2: Schematic diagram indicating positions of principal maxima on the DPPG subgel diffraction pattern and the effects of disorientation. (Left side) centers of broad maxima along the lattice lines are indicated by circles. Indices of lattice lines are given above or below each line. Within each multilayer, the crystalline arrays in the parallel bilayers are assumed to be randomly oriented; this type of disorientation gives rise to concentric cylinders of diffracting power in reciprocal space. The slight curvatures of the lines shown here (both toward the meridian and away from it) are the result of first intersecting the reciprocal-space cylinders with the sphere of reflection and then projecting the intersections onto the flat X-ray film. (Middle) sharp arcs along the (0, 0) lattice line. The radial sharpness is imposed by stacking of bilayers within each multilayer. The arc lengths here and in the right half of the figure are a direct indication of the varying orientations of different multilayers within the specimen, i.e., a second type of disorientation, with a 15° fwhm. (Right side) effect of the 15° disorientation on the broad maxima along the lattice lines. Before introducing the multilayer disorientation, each maximum was represented by a line segment of length equal to the estimated fwhm of the maximum, along the lattice line. Note how the maxima near the equatorial axis, which extend for some distance along their respective lattice lines, nonetheless generate sharp arcs while similar maxima well off this axis give rise to arcs broadened in the radial direction.

& Perutz, 1952), applied to a diffracting specimen of known thickness, t, sets the minimum distance between intensity maxima as approximately $1/t$. Larger separations than $1/t$ can, of course, occur; these would correspond to major substructures separated by less than t. The most closely spaced intensity maxima along the lattice lines are separated by a distance of $\simeq$0.022 Å^{-1} (see Table II). This would set $t \simeq$ 45 Å, a distance consistent with the head group–head group distance across the DPPG bilayer (Figure 5).

Figure 2 shows the predicted effect on the lattice lines due to the varying orientation of the stacked bilayers in the specimen. Note that each point (●) in the left half of Figure 2 represents the peak intensity of a broad maximum along its lattice line. One result of the disorientation is that the broad maxima along any given lattice line sweep out arcs of intensity having different radial widths (right half of Figure 2). The width increases with the vertical distance from the equator to each maximum. Thus, an intensity maximum far from the equator will sweep out an arc that is both wider radially and longer tangentially than a similar maximum on the equator. This explains why the off-equatorial bands are significantly more diffuse than the sharp equatorial reflections in Figure 2 and why there is a mixture of sharp and broad wide-angle bands in unoriented or partially oriented patterns (Wilkinson & McIntosh, 1986).

A final important point to make concerning the wide-angle reflections in Figure 1 relates to lipid chain tilt. For an

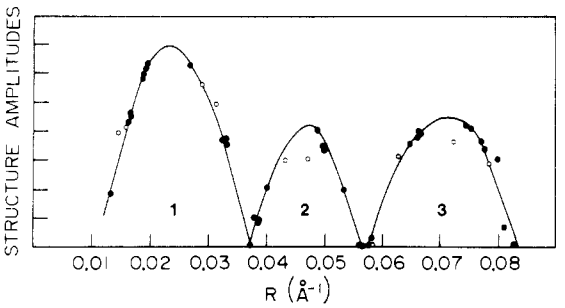

FIGURE 3: Structure amplitudes of lamellar diffraction data for DPPG at 20 °C with no low-temperature incubation (open circles) and at 10 °C after incubation at 4 °C for at least 2 weeks (solid circles). The three regions of the transform are labeled 1–3. The line was drawn by eye through the solid circles.

elongated diffracting unit, such as a lipid molecule with extended hydrocarbon chains, the intensity is expected to be concentrated in a plane perpendicular to the long axis of the chains. If the chains were tilted relative to the plane of the bilayer, then much of the scattering from these chains would be oriented off the equator. In fact, several of the most intense wide-angle maxima (Figure 1B) lie on radii tilted by 20–30° from the equatorial axis.

Analysis of the Lamellar Diffraction. To determine phase angles of the lamellar reflections, a series of swelling experiments was performed by varying the water content in unoriented specimens. Figure 3 shows the structure amplitudes (solid circles) vs. reciprocal space coordinate for eight different specimens with repeat periods ranging from 51.5 to 75.2 Å. The lamellar diffraction extends to about 4 Å for the smaller repeat periods and to about 12 Å for the larger repeat periods. Therefore, the swelling experiments are useful in determining the phase angles to 12-Å resolution. The continuous transform has three peaks, centered at about 0.023, 0.047, and 0.071 $Å^{-1}$, which are labeled 1–3, respectively. Since these specimens are centrosymmetric, each of these transform regions can have a phase angle of either 0 or π. Thus, there are $2^3 = 8$ possible phase combinations. As was done previously (McIntosh et al., 1983, 1984), sampling theorem analysis (Boyes-Watson & Perutz, 1943) was applied to determine which combination best fits all of the structure amplitudes. The structure factor at $R = 0$ was determined by the method of Blaurock (1967) and King & Worthington (1971), and continuous transforms were calculated for each possible phase combination for two data sets, with repeat periods of $d = 51.8$ Å and $d = 75.2$ Å. For the correct phase choice, the continuous transforms calculated for each data set should be the same, within experimental uncertainty. The two curves plotted in each graph in Figure 4 represent the absolute values of the continuous transform for these two data sets. In Figure 4A, alternate phases for regions 1–3 of the transform are shown; in Figure 4B, regions 1 and 2 have the opposite phase of region 3; in Figure 4C, regions 2 and 3 have the opposite phase of region 1; in Figure 4D, all regions have the same phase. Clearly, the two curves in Figure 4A are much closer to one another than the pairs of curves in panels B–D of Figure 4. Thus, the correct phase choice is either $(0, \pi, 0)$ or $(\pi, 0, \pi)$ for the three regions of the transform. The combination $(\pi, 0, \pi)$ was chosen on the basis of the assumption that the hydrocarbon core of the bilayer should have a lower electron density than the head group region.

A typical electron-density profile for the subgel phase with repeat period $d = 75.2$ Å is shown in Figure 5B. A profile for DPPG in the $L_{\beta'}$ phase is shown for comparison in Figure 5A. The same phase combination was used to calculate this

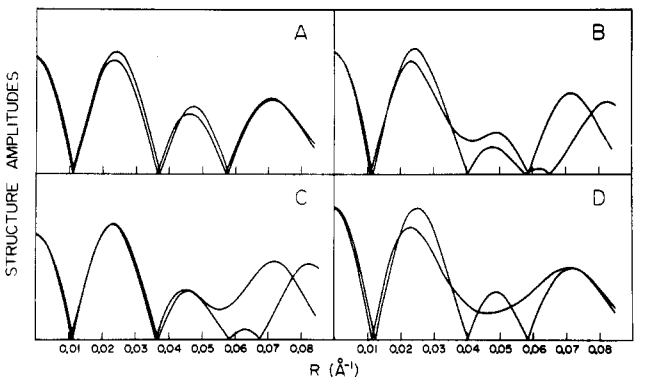

FIGURE 4: Absolute values of continuous transforms calculated by applying the sampling theorem to two data sets with repeat periods of $d = 51.8$ Å and $d = 75.2$ Å. The transform pairs were calculated for (A) alternating phases for regions 1–3, (B) regions 1 and 2 with the opposite phase of region 3, (C) regions 2 and 3 with the opposite phase of region 1, and (D) regions 1–3 all with the same phase.

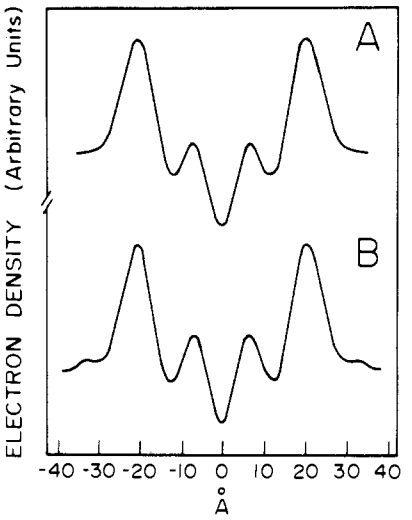

FIGURE 5: Electron-density profiles for DPPG (A) in the $L_{\beta'}$ phase at 20 °C and (B) in the subgel phase at 10 °C after incubation at 4 °C for 2 weeks. Phase angles were chosen as described in the text. The resolution of each profile is about 13 Å.

profile since the structure factors for the $L_{\beta'}$ phase (open circles) fall quite close to the continuous transform of the subgel phase (Figure 3).

The 12-Å resolution profiles for the $L_{\beta'}$ phase (Figure 5A) and the subgel phase (Figure 5B) are very similar in shape. Both profiles are consistent with a bilayer having ordered and tilted hydrocarbon chains. In each profile the high-density peaks, centered at about ±21 Å, correspond to the lipid head groups, the low-density dip at 0 Å corresponds to the terminal methyl groups in the geometric center of the bilayer, and the medium-density region between the head group peaks and the terminal methyl trough corresponds to the lipid methylene chains. The medium-density regions at the outer edges of each profile represent the fluid spaces between adjacent bilayers. Specimens with relatively large repeat periods were used in this figure because the fluid space is more easily observed than in the samples with smaller repeat periods. However, the shape of the bilayer profile itself is quite similar for all water contents. The bilayer thickness for DPPG, as measured by the separation between lipid head group peaks in the electron-density profiles, is much the same for $L_{\beta'}$ and subgel phases: 41.5 ± 0.7 Å (two specimens) for the $L_{\beta'}$ phase and 41.6 ± 1.2 Å (eight specimens) for the subgel phase. From molecular packing models, a 49-Å separation between head groups is expected for DPPG

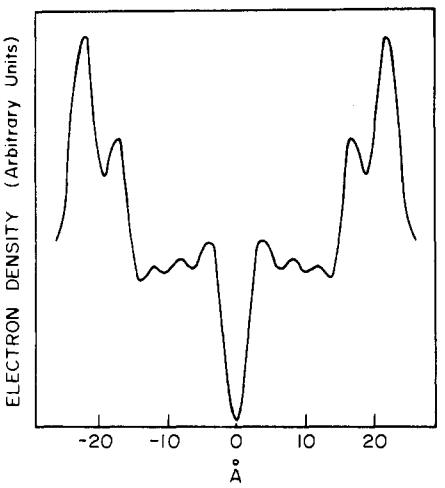

FIGURE 6: A 4.3-Å resolution electron-density profile for DPPG in the subgel phase. Phase angles were chosen as described in the text.

bilayers where the hydrocarbon chains are untilted, that is, perpendicular to the plane of the bilayer. Moreover, for DPPE bilayers and DPPC:tetradecane bilayers that have no chain tilt, the head group separation is about 49 Å in profiles at comparable resolution (McIntosh, 1980). In comparison, DPPC bilayers that have their hydrocarbon chains tilted at an angle of about 30° to the normal to the bilayer have a head group separation of about 42 Å (McIntosh, 1980). Thus, these electron-density profiles show that the DPPG molecules have approximately the same chain tilt in the subgel phase and in the $L_{\beta'}$ phase.

An electron-density profile calculated at about 4-Å resolution by using the higher order reflections for a low water content specimen with $d = 51.5$ Å is shown in Figure 6. The phases for the diffraction orders 5–12 were chosen to give the most uniform electron density for the methylene chain portion of the profile. This criterion, which has been used previously (Wilkins, 1972; Torbet & Wilkins, 1976; Worthington & Khare, 1978), is consistent with the polyethylene-like chain packing indicated for the subgel phase (see Discussion). A similar criterion, applied to the uniform regions of water between protein molecules, has proven to be a powerful constraint on phasing the reflections from protein crystals (Burlingame et al., 1985). In the profile, the terminal methyl trough in the geometric center of the bilayer is quite sharp, and each head group region consists of two peaks, with the outer one being of higher density. This profile is very similar to ones derived for DPPC (Lesslauer et al., 1972; Torbet & Wilkins, 1976; McIntosh, 1978), where the highest density peak in the head group region has been assigned to the phosphate moiety and the inner peak in the head group region has been assigned to the glycerol backbone (Lesslauer et al., 1972; Wilkins, 1972; Torbet & Wilkins, 1976).

Discussion

The X-ray analysis presented in this paper provides for the first time a detailed description of molecular structure in the subgel phase and of the changes in molecular organization that take place at the subgel to gel transition. The electron-density profiles for the $L_{\beta'}$ phase (Figure 5A) and subgel phase (Figure 5B) are very similar, showing that the bilayer thickness and thus the hydrocarbon chain tilt are nearly the same for these two phases. In both phases the spacings and relative intensities of wide-angle reflections are independent of the lamellar stacking distance (Wilkinson & McIntosh, 1986). This indicates that, for both the $L_{\beta'}$ and subgel phases, the molecular packing in each bilayer is independent of adjacent bilayers. However, the molecular packing characteristics are quite different for these two phases. In the $L_{\beta'}$ phase the hydrocarbon chains are packed in a "quasi-hexagonal" array, similar to the array in the saturated phosphatidylcholines (Tardieu et al., 1973). Since the area of the quasi-hexagonal unit cell corresponds to the area of a single hydrocarbon chain, and not the entire diacyl lipid molecule, the position of the head group in the $L_{\beta'}$ phase is not ordered (Tardieu et al., 1973). Rather, the extended hydrocarbon chains are organized with rotational disorder. In contrast, in the DPPG subgel phase, the wide-angle lattice lines indicate a unit cell of area 43.0 Å^2, consistent with the area for an entire lipid molecule with tilted hydrocarbon chains (see below). Thus, the wide-angle reflections from the $L_{\beta'}$ phase relate to the chains alone, which are rotationally disordered, whereas the reflections from the subgel phase (Figure 1) come from crystalline arrays of the entire DPPG molecules (two chains plus head group), each crystalline array being no more than two molecules thick.

Other evidence supporting the conclusion that the crystalline array is one bilayer thick in the subgel phase is the intensity distribution along the wide-angle lattice lines in Figure 1. If the DPPG molecules were organized in three-dimensional crystals, each lattice line would be sampled at the three-dimensional reciprocal lattice points and there would be sharp, arced reflections along each of these lattice lines with the same separation as the lamellar reflections along the meridian. However, in our patterns we observe many broad arcs along the wide-angle lattice lines (Figure 1), indicating that we do not have a three-dimensional crystal but rather stacks of thin, two-dimensional crystals. Along the lattice lines, the smallest distance between maxima corresponds to the head group separation across a bilayer. This is consistent with the diffracting unit being two molecules (one bilayer), rather than one molecule (one monolayer), thick.

In the DPPG subgel phase, the packing of the hydrocarbon chains in the direction normal to the chains bears a marked similarity to the packing in crystalline *n*-alkanes and polyethylene. For both the crystalline *n*-alkanes and polyethylene, the arrays of chains give rise to intense diffraction in the plane perpendicular to the chain axes; the two dominant reflections have Bragg spacings of 4.11 and 3.70 Å (Muller, 1932; Bunn, 1939). Other strong reflections have spacings of 2.96, 2.47, and 2.20 Å (Bunn, 1939). Strong reflections with similar Bragg spacings are present in the DPPG subgel pattern (Tables I and II), indicating similar chain packing for DPPG and the crystalline *n*-alkanes and polyethylene.

One important difference between the chain packing for subgel DPPG and the crystalline *n*-alkanes and polyethylene is the chain tilt in DPPG. There are several lines of evidence that indicate that in the subgel phase the DPPG chains are tilted by 30–35° from the bilayer normal. First, the bilayer thickness, as determined from electron-density profiles (Figure 5B), is smaller than would be expected for fully extended chains oriented perpendicular to the interface. Molecular model calculations and comparisons to electron-density profiles of DPPC bilayers with tilted and untilted chains (McIntosh, 1980) indicate a chain tilt of 30–35° for subgel DPPG. Second, several of the most intense maxima in the oriented diffraction pattern of Figure 1 are located well off the equatorial axis. For example, three of the most intense maxima lie along the (1, −1) and (1, 1) lattice lines and have Bragg spacings from 4.0 to 4.1 Å, and a fourth maximum lies along the (0, 2) line at 3.75 Å. The angles between the in-plane axis and radial lines from the center of the pattern to these maxima are 0, 14, 18, and 34°. If, on the basis of Bragg spacings, we

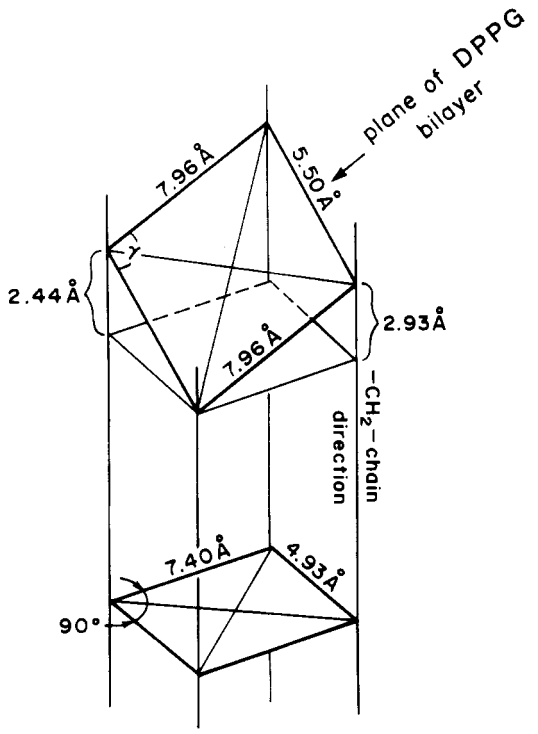

FIGURE 7: Schematic diagram relating the chain packing in DPPG to that in polyethylene. In the latter, four chains pass through the corners of a rectangle 4.93 by 7.40 Å; a fifth chain (not indicated) passes through the center of the rectangle. The DPPG unit cell is generated by cutting obliquely through the parallelepiped determined by the axes of the chains. The dihedral angle between the plane of the rectangle and the DPPG bilayer equals the chain tilt angle, θ. If the rectangle is 4.93 by 7.40 Å, as shown, then $\gamma = 99.4°$ and $\theta = 32°$, while shrinking the rectangle to 4.88 by 7.32 Å (see text) makes $\gamma = 100.5°$, as observed, and $\theta = 34°$.

identify these maxima with the dominant reflections in the plane perpendicular to the chains, then the off-axis location of these maxima clearly indicates tilted chains. The indicated angle of tilt would be at least as great as the largest angle, i.e., the estimated tilt angle on the basis of these reflections is $\geq 34°$. A third indication of tilt is, as discussed in the next paragraph, that the unit-cell dimensions for DPPG are similar to those of polyethylene and the crystalline *n*-alkanes when the chain tilt of 30–35° for DPPG is taken into account.

In the normal form of the crystalline *n*-alkanes, there are two chains in a unit cell with a rectangular cross section in the plane perpendicular to the chain axes (Muller, 1932). The sides of the rectangle depend slightly on the chain length of the alkane and range from 7.3 to 7.4 Å and 4.9 to 5.0 Å. In the case of polyethylene, Bunn (1939) determined an orthorhombic subcell having two chains in a rectangular cross section 7.40 by 4.93 Å; the third dimension of the subcell, 2.53 Å along the chain axis, corresponds to the height of two $-CH_2-$ groups. Thus, the hydrocarbon chains in the crystalline *n*-alkanes or in polyethylene define a rectangular parallelepiped (Figure 7). Because of chain tilt, in DPPG the plane of the bilayer would cut obliquely through such a rectangular parallelepiped giving an oblique unit cell. As shown schematically in Figure 7, the parallelepiped can be cut at a chain tilt angle of 32° in such a way that an oblique lattice is obtained with dimensions $a = 5.50$ Å, $b = 7.96$ Å, and $\gamma = 99.4°$. These dimensions correspond closely to our observed oblique lattice for DPPG of $a = 5.50$ Å, $b = 7.96$ Å, and $\gamma = 100.5°$. Given the latter values, each DPPG chain has four nearest neighbors in the plane perpendicular to the chain axes at a separation of 4.40 Å at 10 °C. This compares to the 4.45-Å distance in Bunn's (1939) polyethylene structure determined at room temperature. The agreement is even more satisfactory when one takes into account that chain separation increases with temperature (Muller, 1932); in this case, γ can be made equal to 100.5°, as observed, by shrinking the polyethylene rectangle to 7.32 by 4.88 Å. The 4.40-Å separation between any chain and its four nearest neighbors in the subgel phase is considerably smaller than the chain separation in the normal $L_{\beta'}$ phase. In the $L_{\beta'}$ phase of DPPC, Tardieu et al. (1973) calculate each hydrocarbon chain has four neighbors at a distance of 4.82 Å and two neighbors at a distance of 4.75 Å.

In the DPPG subgel phase, the hydrocarbon chains evidently tilt for the same reason they do in the $L_{\beta'}$ phase. That is, the DPPG head group has a larger excluded area in the plane of the bilayer than do the hydrocarbon chains. To optimize van der Waal's interactions, the chains tilt cooperatively (McIntosh, 1980).

Ranck et al. (1977) observed a polyethylene-like packing in DPPG at −11 °C. However, that structure is quite different than the subgel phase, as it contains interdigitated hydrocarbon chains oriented perpendicular to the plane of the bilayer. In addition, the unit cell is somewhat larger than in polyethylene.

A key step in interpretation of the nonlamellar wide-angle diffraction from the DPPG subgel structure was obtaining diffraction patterns, such as shown in Figure 1, from highly oriented specimens. In unoriented specimens, there is a mixture of sharp and broad nonlamellar reflections, with many more reflections than can be indexed as reciprocal lattice points in a two-dimensional lattice having reasonable dimensions (Wilkinson & McIntosh, 1986). The oriented pattern (Figure 1) allowed us to demonstrate that the sharp reflections fall on the equator, whereas the broader bands lie off the equator along the lattice lines. The sharp equatorial reflections define the two-dimensional lattice points and in the case of DPPG show that the lattice is oblique. Wide-angle patterns have been obtained from the subgel phase of a variety of symmetric and mixed-chain phosphatidylcholines (Ruocco & Shipley, 1982; Stumpel et al., 1983) and phosphatidylethanolamines (Seddon et al., 1983; Mulukutla & Shipley, 1984). Since these patterns also contain a mixture of sharp and broad wide-angle reflections, this type of structural analysis might also apply to those systems.

Given the beginnings of a molecular packing analysis presented here, bond-length data, and the wealth of information in the off-equatorial diffraction in Figure 1, it may prove possible to refine a structure for the DPPG molecule in the subgel phase.

ACKNOWLEDGMENTS

We thank Dr. Allan Wilkinson for drawing this interesting problem to our attention, Dr. William Longley for many helpful discussions, and Belinda Irsula for typing the manuscript.

Registry No. DPPG, 4537-77-3; polyethylene, 9002-88-4.

REFERENCES

Blaurock, A. E. (1967) Ph.D. Thesis, University of Michigan.
Blaurock, A. E. (1982) *Methods Enzymol. 88*, 124–132.
Blaurock, A. E., & Stoeckenius, W. (1971) *Nature (London), New Biol. 233*, 152–155.
Bragg, W. L., & Perutz, M. F. (1952) *Proc. R. Soc. London, Ser. A 213*, 425–435.
Bunn, C. W. (1939) *Trans. Faraday Soc. 35*, 482–491.
Burlingame, R. W., Love, W. E., Wang, B.-C, Hamlin, R., Xuong, N.-H., & Moudrianakis, E. N. (1985) *Science (Washington, D.C.) 228*, 546–553.

Fuldner, H. H. (1981) *Biochemistry 20*, 5707–5710.
Hahn, T. (1983) *International Tables for Crystallography*, Vol. A, pp 82–83, D. Reidel, Boston.
Henderson, R., & Unwin, P. N. T. (1975) *Nature (London) 257*, 28–32.
King, G. I., & Worthington, C. R. (1971) *Phys. Lett. 35A*, 259.
Lesslauer, W., Cain, J. E., & Blasie, J. K. (1972) *Proc. Natl. Acad. Sci. U.S.A. 69*, 1499–1503.
McIntosh, T. J. (1978) *Biochim. Biophys. Acta 513*, 43–58.
McIntosh, T. J. (1980) *Biophys. J. 29*, 237–246.
McIntosh, T. J., McDaniel, R. V., & Simon, S. A. (1983) *Biochim. Biophys. Acta 731*, 109–114.
McIntosh, T. J., Simon, S. A., Ellington, J. C., & Porter, N. A. (1984) *Biochemistry 23*, 4038–4044.
Muller, A. (1932) *Proc. R. Soc. London, Ser. A 138*, 514–530.
Mulukutla, S., & Shipley, G. G. (1984) *Biochemistry 23*, 2514–2519.
Ranck, J. L., Keira, T., & Luzzati, V. (1977) *Biochim. Biophys. Acta 488*, 432–441.
Ruocco, M. I., & Shipley, G. G. (1982) *Biochim. Biophys. Acta 684*, 59–66.
Seddon, J. M., Harlos, K., & Marsh, D. (1983) *J. Biol. Chem. 258*, 3850–3854.
Shannon, C. E. (1949) *Proc. Inst. Radio. Eng. N.Y. 37*, 10–21.
Stumpel, J., Eibl, H., & Nicksch, A. (1983) *Biochim. Biophys. Acta 727*, 246–254.
Tardieu, A., Luzzati, V., & Reman, F. C. (1973) *J. Mol. Biol. 75*, 711–733.
Torbet, J., & Wilkins, M. H. F. (1976) *J. Theor. Biol. 62*, 447–458.
Wilkins, M. H. F. (1972) *Ann. N.Y. Acad. Sci. 195*, 291–292.
Wilkinson, A., & McIntosh, T. J. (1986) *Biochemistry* (previous paper in this issue).
Worthington, C. R., & Khare, R. S. (1978) *Biophys. J. 23*, 407–425.

Glucose-Specific Permease of the Bacterial Phosphotransferase System: Phosphorylation and Oligomeric Structure of the Glucose-Specific II^{Glc}–III^{Glc} Complex of *Salmonella typhimurium*†

Bernhard Erni

Department of Microbiology, Biocenter of the University of Basel, CH-4056 Basel, Switzerland

Received July 18, 1985

ABSTRACT: The glucose-specific membrane permease (II^{Glc}) of the bacterial phosphoenolpyruvate-dependent phosphotransferase system (PTS) mediates active transport and concomitant phosphorylation of glucose. The purified permease has been phosphorylated in vitro and has been isolated (P-II^{Glc}). A phosphate to protein stoichiometry of between 0.6 and 0.8 has been measured. Phosphoryl transfer from P-II^{Glc} to glucose has been demonstrated. This process is, however, slow and accompanied by hydrolysis of the phosphoprotein unless III^{Glc}, the cytoplasmic phosphoryl carrier protein specific to the glucose permease (II^{Glc}) of the PTS, is added. Addition of unphosphorylated III^{Glc} resulted in rapid formation of glucose 6-phosphate with almost no hydrolysis of P-II^{Glc} accompanying the process. A complex of II^{Glc} and III^{Glc} could be precipitated from bacterial cell lysates with monoclonal anti-II^{Glc} immunoglobulin. The molar ratio of II^{Glc}:III^{Glc} in the immunoprecipitate was approximately 1:2. Analytical equilibrium centrifugation as well as chemical cross-linking showed that purified II^{Glc} itself is a dimer (106 kDa), consisting of two identical subunits. These results suggest that the functional glucose-specific permease complex comprises a membrane-spanning homodimer of II^{Glc} to which four molecules of III^{Glc} are bound on the cytoplasmic face.

The bacterial phosphotransferase system (PTS)[1] comprises a number of proteins with interdependent metabolic and regulatory functions. One primary function is the active uptake of sugars and hexitols. Depending on the availability of these substrates, components of the PTS regulate the uptake of nutrients through other transport systems [by inducer exclusion and/or by regulation of gene expression; for reviews, see Postma & Roseman (1976) and Saier (1977, 1985)]. A functional PTS is further required for PTS substrate-directed chemotaxis (Adler & Epstein, 1974; Niwano & Taylor, 1982). Genetic and biochemical analysis revealed that the PTS consists of two cytoplasmic proteins and several membrane permeases with different sugar specificities. The permease proteins (enzymes II) span the cytoplasmic membrane, mediating sugar transport concomitant with sugar phosphorylation. As depicted schematically in Figure 1, the cytoplasmic proteins, enzyme I and HPr, are the phosphoryl carriers that transfer phosphoryl groups sequentially from phosphoenolpyruvate to the sugars in an enzyme II dependent reaction. Uptake of glucose in particular requires a third cytoplasmic protein, designated III^{Glc}. It functions as the phosphoryl carrier

† This study was supported by Grant 3.527-0.83 from the Swiss National Science Foundation.

[1] Abbreviations: PTS, phosphoenolpyruvate sugar–phosphotransferase system; enzyme I, enzyme I of the PTS; HPr, histidine-containing phosphocarrier protein of the PTS; P-II^{Glc}, phosphorylated form of the glucose-specific enzyme II of the PTS; P-III^{Glc}, phosphorylated form of the glucose-specific enzyme III of the PTS; αMG, methyl α-glucopyranoside; octyl-POE, polydisperse octyloligo(oxyethylene); Glc-6-P, glucose 6-phosphate.

0006-2960/86/0425-0305$01.50/0